Digest Journal of Nanomaterials and Biostructures Vol. 19, No. 4, October-December 2024, p. 1435-1447

Synthesis and sensing characterizations of nanostructured tin-doped Fe_2O_3 thin films

E. K. Jassem [a], O. A. Chichan [b], M. F. Allawai [c], K. N. Hussein [d], S. S. Chiad [e], N. F. Habubi [f], Y. H. Kadhim [g] M. Jadan [h, i,*]

[a]*Audiology and speech department, Institute of medical Technology-Baghdad, Middle Technical university, Iraq*

[b]*Department of Physics, College of Education for Pure Sciences, University of Babylon, Iraq*

[c]*Department of medical physics, College of Applied Science, University of Fallujah, Iraq*

[d]*Department of Radiology, Al-Manara College for Medical Science, Iraq*

[e]*Department of Physics, College of Education, Mustansiriyah University, Iraq*

[f]*Department of Radiology and Sonar Techniques, Alnukhba University College, Baghdad 10013, Iraq*

[g]*Department of Optics Techniques, College of Haelth and Medical Techniques, AL-Mustaqbal University, Babylon, Hillah, 51001, Iraq*

[h]*Department of Physics, College of Science, Imam Abdulrahman Bin Faisal University, P.O. Box 1982, 31441 Dammam, Saudi Arabia*

[i]*Basic and Applied Scientific Research Center, Imam Abdulrahman Bin Faisal University, P.O. Box 1982, 31441 Dammam, Saudi Arabia*

Nanostructured Tin-doped Fe_2O_3 with a volumetric concentration of (1% and 3 %) Tin were deposited using spray pyrolysis (SPM). The most substantial peak, as determined by X-ray diffraction, corresponds to the (200). The average particle size values from AFM imaging for the deposited films decreased from 81.52 nm to 40.05 nm. The average roughness was observed to drop from 8.26 nm to 45.38 nm. The Root mean square roughness was lowered from 7.48 nm to 4.86 nm. The strain decreases from (27.92 to 23.69) $x10^{-4}$. SEM images show morphological changes in Fe_2O_3 film's big islands after Tin doping. The optical transmittance is outstanding for Undoped Fe_2O_3 and 3% Sn doping, with 80% and 75 %in the visible zone. It was shown that the absorption coefficient increased as the concentration of Tin was raised. The Fe_2O_3 bandgap was reduced from 2.80 eV for Fe_2O_3 to 2.60 eV for Fe_2O_3: 3 % Sn film. Resistance in Fe_2O_3 and Tin-doped films rises in NO_2 (270 ppm) exposure, indicating an oxidation process. The 3% Tin-doped film shows the highest resistance. Sensitivity declined with increasing Tin content following NO_2 exposure.

(Received June 18, 2024; Accepted October 7, 2024)

Keywords: Fe_2O_3, Sn, Thin films, XRD, AFM, SEM, Optical properties, bandgap, Sensitivity

1. Introduction

The advancement of science, particularly in nanotechnology, has underscored the significance of metal oxide materials in various applications [1]. Metal oxides can be engineered to exhibit both p-type and n-type conductivity [2], enhancing their versatility in nanotechnological applications. The transition metal Fe_2O_3 has a band gap of 2.2 eV, making it crucial [3]. Due to its beneficial inherent physical and chemical characteristics, including cheap cost, stability under natural conditions, and kindness to the environment are all attractive qualities. [4], it has attracted a lot of interest. Photoelectrodes, gas sensing, catalysts, and medical sectors all use (Fe_2O_3). Therefore, the material with the most significant potential for usage in a wide range of optical applications and technologies is iron oxide, which is used in telecommunication, electrochromic applications, and

* Corresponding author: muhannadjadan99@gmail.com
https://doi.org/10.15251/DJNB.2024.194.1435

magnetic devices. [5]. Microelectronic devices also use thin layers of Fe_2O_3 as a dielectric material [6]. Hematite, a stable form of iron oxide, can be utilized in photoelectrodes, photovoltaic applications and devices, solar energy conversion, magnetic and nonlinear optical devices, sensors, and other objects [7-9]. Researchers prepare hematite nanostructures using several methods to deposit nanostructure films [10-17], and also use the Chemical deposition [18], sol-gel [19, 20], and PLD [21] ,CVD [22], thermal evaporation method [23], DC reactive magnetron sputtering [24], and SPM [25] techniques to obtain Fe_2O_3 . This paper explores the physical properties of nanostructured Fe_2O_3 and Fe_2O_3: Sn films deposited using the Spray Pyrolysis Method. It is simple, easy to use, and inexpensive.

2. Experimental

The Spray Pyrolysis Method made undoped Fe_2O_3 and Fe_2O_3: Sn thin films. The initial stock solution was employed using Fe chloride in deionized water at 0.05 M. 0.05 M of $SnCl_2$ resolved in deionized water was added as a dopant. A few drops of HCl were added to obtain the solution transparency that was agitated for 8 minutes. Tin had a volumetric ratio of (1, 3) %, and the base temperature was 450 ºC. The layers were placed onto glass bases after chemically and ultrasonically cleaned. To optimize the deposition, the following parameters were used: 5 ml/ moin deposition rate, distance between base to spout was 28 cm , 8 sec of spraying duration per cycle, 1.5 min between sprays, and carrier gas is (pressurized filter air) at a pressure of 10^5 Nm^{-2}. The approximate thickness was found to be 250 nm using the gravimetric method. An X-ray diffractometer (Shimadzu Japan) examined the deposited film structure. X-ray diffractometer (XRD) with CuKα radiation was applied to specify the structure's composition. The film surface was studied using AFM (AA 3000 Scanning Probe Microscope). SEM images were obtained using model ALS 2300 Angstrom. The optical properties of Fe_2O_3 and Fe_2O_3: Sn films were evaluated with a double beam spectrophotometer UV-Vis-NIR Shimadzu. The gas sensor, consisting of undoped Fe_2O_3 and Tin-doped Fe_2O_3, was constructed with Al electrodes. Gas sensitivity was assessed by measuring the change in resistance within a cylindrical chamber with a radius of 8 cm and a height of 16 cm.

3. Results and discussions

XRD patterns of the intended films, grown via the spray pyrolysis method, are presented in Figure 1. The identified diffraction peaks at angles (28.23°, 32.96°, 56.01°, and 64.35°) correspond to the crystallographic planes (111), (200), (211), and (321), respectively. These observations are consistent with ICDD card number 42-1340 [26]. The presence of these diffraction peaks indicates the crystalline nature of the films and provides insights into their preferred crystallographic orientations [27-29].

Using Scherrer formula given in Eq, 1, the grain size of Fe_2O_3 thin films was estimated [30]:

$$D = \frac{k\lambda}{\beta cos\theta} \tag{1}$$

Where λ is the x-ray wavelength, k = 0.9, and θ is Bragg's angle. The grain size for undoped Fe_2O_3 particles is about (12.40-14.57) nm, and with the addition of 3% Sn, the grain size is expected to remain within this range. The particular values point to the impact of Sn doping on Fe_2O_3 particle grain size [31, 32].

The structural parameters S_p such as dislocation density (δ) was measured using [33]:

$$\delta = \frac{1}{D^2} \tag{2}$$

The information in Table 1 indicates a decrease in dislocation density from 65.03 to 47.10. A decrease in dislocation density can suggest an improvement in the crystalline quality or a reduction in the number of crystal defects within the material. This behavior may be attributed to various factors, such as doping changes in the processing conditions [34, 36].
The films' strain (ε) was ascertained using [37]:

$$\varepsilon = \frac{\beta cos\theta}{4} \tag{3}$$

As can be seen in Table 1, ε dropped from 27.92 to 23.69.

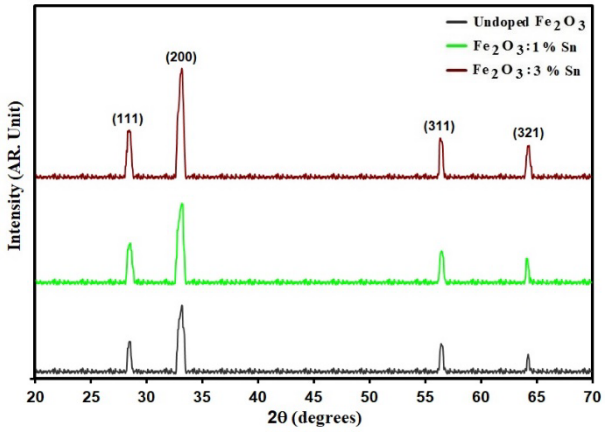

Fig.1. XRD styles of grown films.

Table 1. D, E_g and Sp of grown films.

Sample	2 θ (°)	(hkl) Plane	FWHM (°)	E_g (eV)	*D* (nm)	δ(× 10^{14}) (lines/m^2)	ε(× 10^{-4})
Fe_2O_3	28.23	200	0.66	2.80	12.40	65.03	27.92
Fe_2O_3: 1% Sn	28.26	200	0.60	2.65	13.60	54.06	25.38
Fe_2O_3: 3% Sn	28.29	200	0.56	2.60	14.57	47.10	23.69

The AFM micrographs in Fig. (2) provide insights into the surface morphology of the films. Average Particle Size (Pav) values (81.52, 50.13, 40.05 nm) indicate the average size of surface features. Roughness Average (Ra) values (8.26, 6.91, 5.38 nm) suggest surface smoothness, and Root-Mean-Square Roughness (R_{rms}) values (7.48, 5.93, 4.86 nm) represent height deviations. Table (2) shows further details of AFM parameters (P_{AFM}). These parameters are crucial for understanding and optimizing surface characteristics in applications requiring precise film surfaces, such as various thin-film technologies [38, 39].

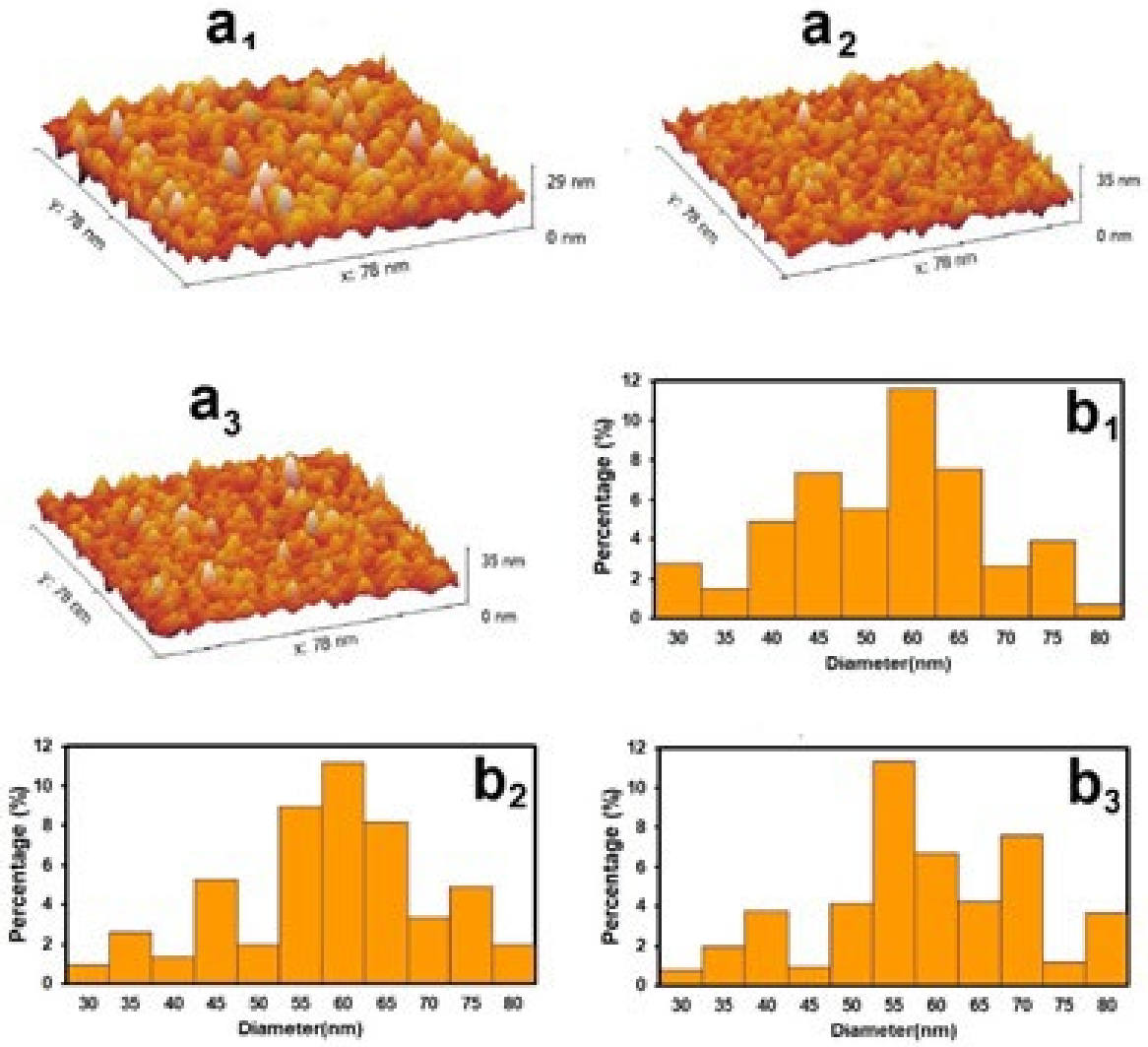

Fig. 2. AFM images, granularly distributed and diversity of PAFM. Fig.2. AFM images , granularly distributed and diversity of PAFM.

Table 2. P_{AFM} of the intended films.

Samples	P_{av} nm	R_a (nm)	R_{rms} (nm)
Fe_2O_3	81.52	8.26	7.48
Fe_2O_3: 1% Sn	50.13	6.91	5.93
Fe_2O_3: 3% Sn	40.05	5.38	4.86

Fig. (3) displays SEM pictures of the synthesized films, which include Undoped Fe_2O_3, Fe_2O_3: 1% Sn, and Fe_2O_3: 3% Sn. The images show a significant change in the shape of artificial films, characterized by a more substantial number of islands following doping. This behaviour is probably caused by the interaction between the Fe_2O_3 matrix and the additional Sn, which affects the formation and organization of nanostructures during the film synthesis process [40, 41].

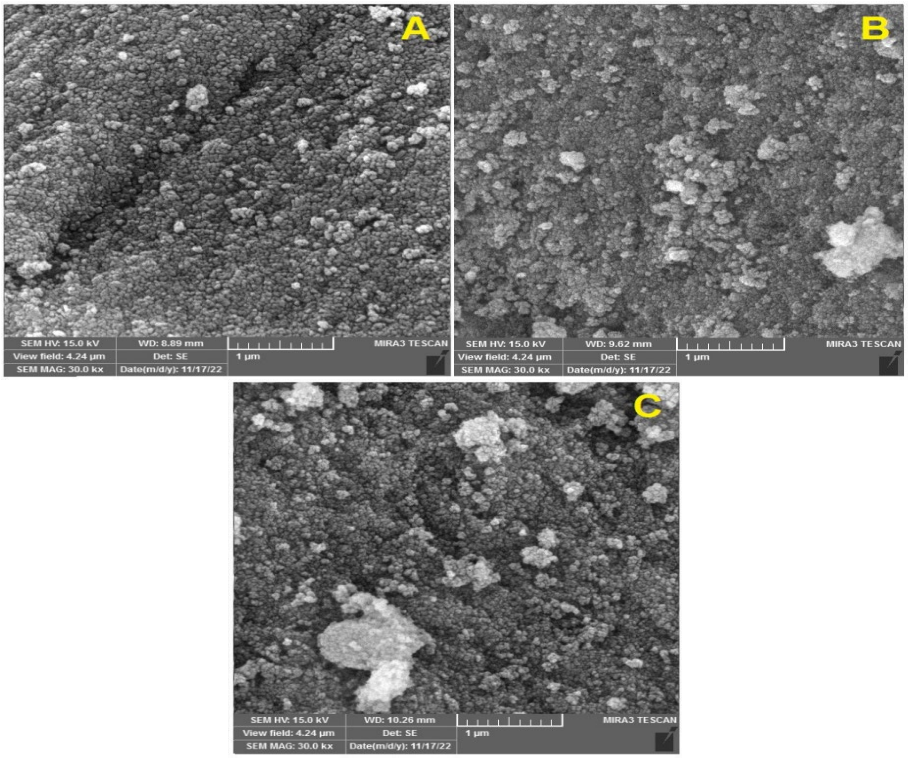

Fig. 3. SEM images of (a) Fe_2O_3 (b) 1% doped by Sn (c) 3% doped by Sn.

Experimental measurements are commonly presented using the transmittance (T), defined as [42]:

$$T\% = \frac{I}{I_o}\% \tag{4}$$

where (I) is the light intensity after it passes through the sample and (Io) is the initial light intensity. The optical transmission spectra in Fig. (4) depict the performance of undoped Fe_2O_3 and Tin-doped Fe_2O_3 films. Both films exhibit robust transmission, exceeding 80% on average at a wavelength of 800 nm. This high transmission is crucial for solar cell applications[43, 44]. The results suggest the potential suitability of these films for applications where optical transparency is essential, emphasizing their promising role in optoelectronic device technologies [45, 46]
The absorbance (A) and thickness (t) were gained to calculate absorption coefficient (α) [48];

$$\alpha = (2.303 \times A)/t \tag{5}$$

Fig. (5) it is evident that the increase in α with the elevated Tin content suggests a notable enhancement in the transitions from bonding molecular orbit to nonbonding molecular orbit. This significant rise in the absorption coefficient, especially at higher energy levels, indicates a change in optical properties. The results point towards the impact of Tin doping influencing their optical characteristics and paving the way for tailored applications in optoelectronics [49, 50].

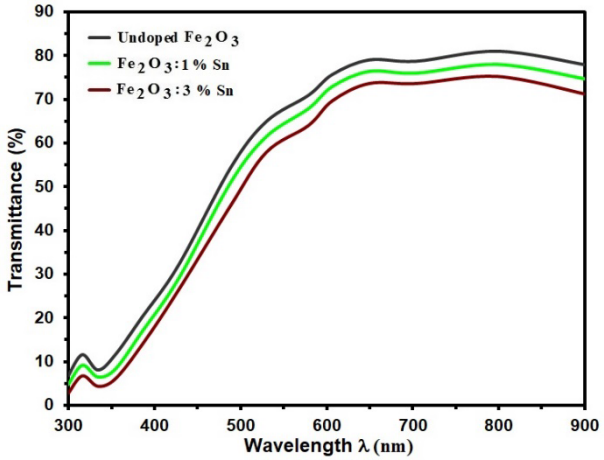

Fig. 4. Transmittance of the deposited Fe_2O_3 and Fe_2O_3: Sn thin films.

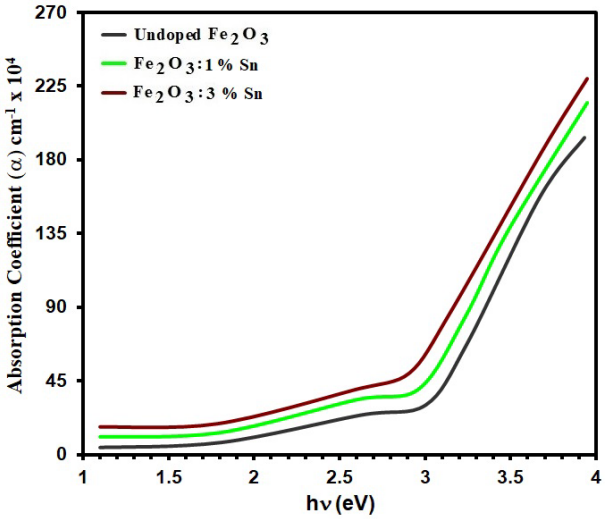

Fig. 5. α of grown films.

The band gap (E_g) is evaluated byTauc 's formula [51]:

$$(\alpha h\nu) = A\left(h\nu - E_g\right)^{\frac{1}{2}} \tag{6}$$

Plots were obtained using A as the constant and $(h\nu)^2$ via (hυ). As depicted in Fig. (6), the bandgap values (E_g) for Undoped Fe_2O_3 and Fe_2O_3: Sn were relatively close. However, there was a reduction in E_g from 2.80 eV - 2.60. This bandgap narrowing signifies a change to the electrical material structure due to the introduction of tin doping [52, 53]. Such changes in the bandgap can influence the material's optical and electronic properties, making it suitable for specific applications, such as semiconductor devices [54, 55].

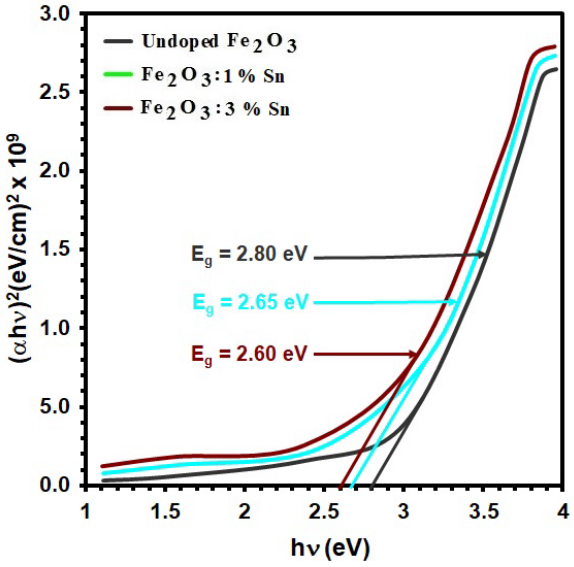

Fig. 6. E_g of deposit films.

The extinction coefficient (k) is gained via Eq. 7 [56]:

$$k = \frac{\alpha\lambda}{4\pi} \tag{7}$$

Where λ is the wavelength, Fig. (7) illustrates the variation in the extinction coefficient (k) with wavelength as the tin dopant concentration increases. The fluctuations in the extinction coefficient provide insights into the material's interactions with light at different wavelengths. The changes in k indicate how introducing tin doping influences the material's optical properties, precisely its absorption characteristics [57, 58].

The refractive index (n) can be determined from the reflectance (R) data via the relation [59]:

$$n = \left(\frac{1+R}{1-R}\right) + \sqrt{\frac{4R}{(1-R)^2} - k^2} \tag{8}$$

As observed in Fig. (8), n is influenced by the content of the tin dopant, showing a decrease as the tin dopant concentration increases. This change in n may be associated with an increase in the film's compactness [60, 61]. n can impact the material's optical behavior.

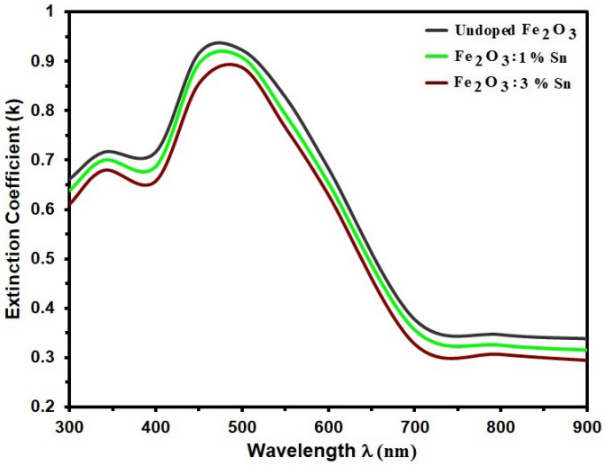

Fig. 7. k of the intended films

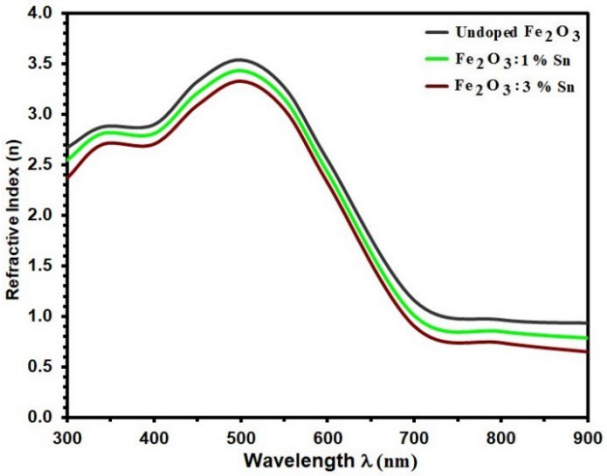

Fig. 8. n of the intended films.

Fig. (9) illustrates the relationship between resistance and time for undoped Fe_2O_3 and Tin-doped films for NO_2 gas concentration of 270 ppm and at an operating temperature of 100 °C. The observed increase in resistance for pure Fe_2O_3 and Tin-doped films when exposed to NO_2 gas suggests an oxidation process. NO_2 molecules adsorb onto the surface, removing specific O^{2+} ions and releasing bound electrons from oxygen atoms [62, 63]. These released electrons then drift back to the conduction band, causing an increase in resistance and an enhancement in the potential barrier [64, 65]. Notably, the film doped with 3% Tin demonstrates the highest resistance to the gas flow, indicating the significant impact of doping on film properties [66].

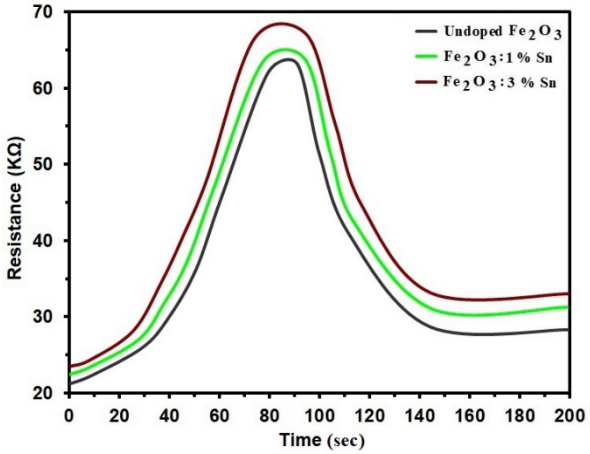

Fig. 9 Resistance via operating time for grown films

The ratio of a film's resistance in air to its steady-state value in the presence of gas is known as its sensitivity (S), and it is typically determined by [67]:

$$Sensitivity = \frac{\Delta R}{R_g} = \left|\frac{R_g - R_a}{R_g}\right| \times 100\ \% \tag{8}$$

When exposed to different amounts of NO_2 gas, as seen in Figure (11). the sensitivity reduces as the Tin content increases. The rising electrical film resistance explains this. The recombination mechanism between the charge carriers of holes and electrons generated from oxygen causes this rise in resistance [68]. The sensitivity shows an increase in its value when the gas concentration rises.

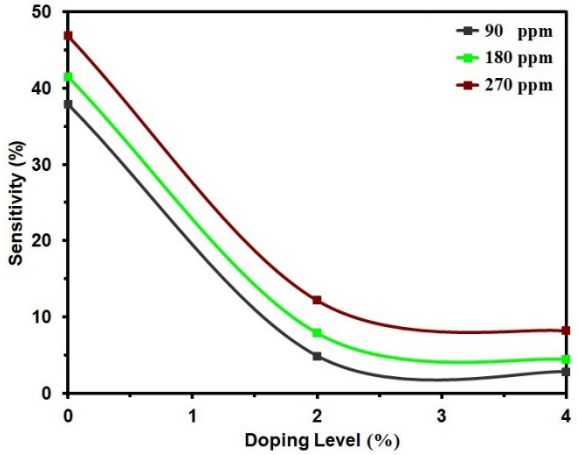

Fig. 10 S via gas concentrationn.

4. Conclusion

The Spray Pyrolysis Method was used to grow undoped Fe_2O_3 films doped with Tin. The shape of Fe_2O_3 thin films changed dramatically as the tin dopant increased from 0% to 3%. According to X-ray diffraction, the optimal orientation (200) for Undoped Fe_2O_3 films at 4 % Sn corresponds to the peak of greatest intensity. With Fe_2O_3: 3% Sn, the grain size for undoped Fe_2O_3 particles is around (12.40 - 14.57) nm, but the strain decrsed from 27.92 to 23.69.

With Undoped Fe_2O_3 and Fe_2O_3: 3% Sn, the average particle size was seen in the area of 81.52 nm to 40.05 nm, respectively. SEM images reveal morphological changes in big islands after Sn doping in Fe_2O_3 films. The transmittance spectra are set by UV-Visible spectrophotometer. With increasing Tin doping, the optical energy gap dropped to 2.60 eV for the Fe_2O_3: 3 % Sn film, but the absorption coefficient increased. The optical constants were also calculated. The increase in resistance for both undoped and Sn-doped films under NO_2 (270 ppm) exposure suggests an oxidation process, with the 3% Tin-doped film exhibiting the highest resistance. Sensitivity decreased with increasing Sn content after NO_2 exposure.

Acknowledgments

Mustansiriyah University and Al-Nukhba University College supported this effort.

References

[1] M. Abaker, U. Ahmad, S. Baskoutas, G.N. Dar, S.A. Zaidi, S.A. Al-Sayari, A. Al-Hajry, S.H.Kim, S.W. Hwang, Journal of Physics D: Applied Physics, 44, 425401(2011); https://doi.org/10.1088/0022-3727/44/42/425401/meta
[2] V. M. Aroutiounian, V.M. Arakelyan, G.E. Shahnazaryan, Solar Energy, 78 (2005) 581-592, https://doi.org/10.1016/j.solener.2004.02.002
[3] C. Wang, L. Yin, L. Zhang, D. Xiang, R. Gao, Sensors, 10 (2010); https://doi.org/10. 10.3390/s100302088
[4] X. Lai, G. Shen, P. Xue, B. Yan, H. Wang, P. Li, W. Xia, J. Fang, Nanoscale, 7, 4005-4012 (2015); https://doi.org/10.1039/C4NR05772D
[5] N. Song, H. Jiang, T. Cui, L. Chang, X. Wang, Nano Letters, Institution of Engineering and Technology, 943-946 (2012); https://doi.org/10.1049/mnl.2012.0631
[6] J. Chen, L. Xu, W. Li, X. Gou, Advanced Materials, 17. 582-586 (2005); https://doi.org/10.1002/adma.200401101
[7] S. S. Chiad, K. H. Abass, T. H. Mubarak, N. F. Habubi, M. K. Mohammed, A. A. , Khadayeir, Journal of Global Pharma Technolog, 11(4), 369-375 (2019).
[8] M. Tadić, D. Marković, V. Spasojević, V. Kusigerski, M. Remškar, J. Pirnat, Z. Jagličić, Journal of Alloys and Compounds, 441, 291-296 (2007); https://doi.org/10.1016/j.jallcom.2006.09.099
[9] M. Zahn, Journal of Nanoparticle Research, 3, 73-78 (2001); https://doi.org/10.1023/A:1011497813424
[10] S. K. Muhammad, M. O. Dawood, N. Y. Ahmed, E. S. Hassan, N. F. Habubi, S. S. Chiad, Journal of Physics: Conference Series, 1660 (1), 012057 (2020); https://doi.org/ 10.1088/1742-6596/1660/1/012057
[11] Bandgar, D., Navale, S., Khuspe, G., Pawar, S., Mulik, R., Patil, V., Materials Science in Semiconductor Processing 17, 67-73 (2014); https://doi.org/10.1016/j.mssp.2013.08.016
[12] Bandgar, D., Navale, S., Mane, A., Gupta, S., Aswal, D., Patil, V., 2015 Synthetic Metals 204, 1-9 (2015); https://doi.org/10.1016/j.synthmet.2015.02.032
[13] Hao, Q., Li, L., Yin, X., Liu, S., Li, Q., Wang, T., Materials Science and Engineering: B 176, 600-605 (2011); https://doi.org/10.1016/j.mseb.2011.02.002
[14] Huo, L., Li, Q., Zhao, H., Yu, L., Gao, S., Zhao, J., Sensors and Actuators B: Chemical 107, 915-920 (2005); https://doi.org/10.1016/j.snb.2004.12.046
[15] Lee, E., Jang, G., Kim, C., Yoon, D., Sensors and Actuators B: Chemical 77, 221-227 (20010); https://doi.org/10.1016/S0925-4005(01)00716-X
[16] Wang, S., Wang, L., Yang, T., Liu, X., Zhang, J., Zhu, B., Zhang, S., Huang, W., Wu, S., Journal of Solid State Chemistry 183, 2869-2876 (2010); https://doi.org/10.1016/j.jssc.2010.09.033
[17] Wang, S., Wang, W., Wang, W., Jiao, Z., Liu, J., Qian, Y., 2000. Sensors and Actuators B: Chemical 69, 22-27 (2000); https://doi.org/10.1016/S0925-4005(00)00304-X

[18] S. Mathur, V. Sivakov, H. Shen, S. Barth, C. Cavelius, A. Nilsson, P.Kuhn, Thin Solid Films. 502 88-93 (2006); https://doi.org/10.1016/j.tsf.2005.07.249
[19] Kan-Rong Lee et al, Int. J. Electrochem. Sci. 9, 7680-7692 (2014); https://doi.org/10.1016/S1452-3981(23)10997-7
[20] C.D. Park, D. Magana, A. E. Chem. Mater. 19, 677-683 (2007); https://doi.org/10.1021/cm0617079
[21] X.W. Li, A. Gupta, G. Xiao, G.Q. Gong, J. Appl. Phys. 83, 7049-7051(1998); https://doi.org/10.1063/1.367547
[22] E.L. Miller, D. Paluselli, B. Marsen, R.E. Rocheleau, Solar Energy Mater. And Solar Cells. 88, 131-144 (2005); https://doi.org/10.1016/j.solmat.2004.07.058
[23] A.Z. Moshfegh, R. Azimirad, O. Akhavan, Thin Solid Films. 484, 124-131 (2005); https://doi.org/10.1016/j.tsf.2005.02.019
[24] J.A. Glasscock, P.R.F. Barnes, I.C. Plumb, N. Savvides, J. Phys. Chem. C 111, 16477-16488 (2007); https://doi.org/10.1016/j.nanoen.2020.105089
[25] Khadayeir, A. A., Hassan, E. S., Mubarak, T. H., Chiad, S.S., Habubi, N. F., Dawood, M.O., Al-Baidhany, I. A., Journal of Physics: Conference Series, 1294 (2) 022009(2019); https://doi.1088/1742-6596/1294/2/022009
[26] A. J. Ghazai, O. M. Abdulmunem, K. Y. Qader, S. S. Chiad, N. F. Habubi, AIP Conference Proceedings 2213 (1), 020101 (2020); https://doi.org/10.1063/5.0000158
[27] H. A. Hussin, R. S. Al-Hasnawy, R. I. Jasim, N. F. Habubi, S. S. Chiad, Journal of Green Engineering, 10(9), 7018-7028 (2020); https://doi.org/10.1088/1742-6596/1999/1/012063
[28] S. S. Chiad, H. A. Noor, O. M. Abdulmunem, N. F. Habubi, M. Jadan, J. S. Addasi, Journal of Ovonic Research, 16 (1), 35-40 (2020). https://doi.org/10.15251/JOR.2020.161.35
[29] H. T. Salloom, E. H. Hadi, N. F. Habubi, S. S. Chiad, M. Jadan, J. S. Addasi, Digest Journal of Nanomaterials and Biostructures, 15 (4), 189-1195 (2020); https://doi.org/10.15251/DJNB.2020.154.1189
[30] R. S Ali, N. A. H. Al Aaraji, E. H. Hadi, N. F. Habubi, S. S. Chiad, Journal of Nanostructuresthis link is disabled, 10(4), 810–816 (2020); https://doi: 10.22052/jns.2020.04.014
[31] F. A. Jasima , Z. S. A. Mosa, N. F. Habubi, Y. H. Kadhim, S. S. Chiad, Digest Journal of Nanomaterials and Biostructures, 18 (3), 1039–1049 (2023); https://doi.org/10.15251/DJNB.2023.183.1039
[32] S. K. Muhammad, N. D. M. Taqi, S. S. Chiad, K. H. Abass, N. F. Habubi, Journal of Green Engineering, 11(2), 1287-1299 (2021).
[33] A. A. Abdul Razaq, F. H. Jasim, S. S. Chiad F. A. Jasim, Z. S. A. Mosa , Y. H. Kadhimd, Journal of Ovonic Research, 20 (2), 131 – 141 (2024); https://doi.org/10.15251/JOR.2024.202.131
[34] E. S. Hassan, D. M. Khudhair, S. K. Muhammad, A. M. Jabbar, M.O. Dawood, N. F. Habubi, S. S. Chiad, Journal of Physics: Conference Series ,1660 (1) 1660 012066 (2020); https://doi.org/10.1088/1742-6596/1660/1/012066
[35] A. S. Al Rawas, M. Y. Slewa, B. A. Bader, N. F. Habubi, S. S. Chiad, Journal of Green Engineering,10 (9), 7141-7153 (2020); https://doi.org/10.1021/acsami.1c00304
[36] R. S. Ali, H. S. Rasheed, N. F. Habubi, S.S. Chiad, Chalcogenide Letters,, 20 (1), 63–72 (2023; https://doi.org/10.15251/CL.2023.201.63
[37] A. S. Alkelaby, K. H. Abass, T. H. Mubarak, N. F. , Habubi, S. S. Chiad, I. Al-Baidhany, Journal of Global Pharma Technology 11(4), 347-352 (2019).
[38] N. Y. Ahmed, B. A. Bader, M. Y. Slewa, N. F. Habubi, S. S. Chiad, NeuroQuantology, 18(6), 55-60 (2020); https://doi.org/10.1016/j.jlumin.2021.118221
[39] A. A. Khadayeir, K. H. Abass, S. S. Chiad, M. K. Mohammed, N. F. Habubi, T. K. Hameed, I. A. Al-Baidhany, Journal of Engineering and Applied Sciences, 13 (22), 9689-9692 (2018).
[40] A. Ghazai, K. Qader, N. F. Hbubi, S. S. Chiad, O. Abdulmunem, IOP Conference Series: Materials Science and Engineering, 870 (1), 012027 (2020); https://doi.org/ 10.1088/1757-899X/870/1/012027
[41] R. S. Ali, M. K. Mohammed, A. A. Khadayeir, Z. M. Abood, N. F. Habubi and S. S. Chiad, Journal of Physics: Conference Series, 1664 (1), 012016 (2020);

https://doi:10.1088/1742-6596/1664/1/012016
[42] A. A. Khadayeir, R. I. Jasim, S. H. Jumaah, N. F, Habubi, S. S. Chiad, Journal of Physics: Conference Series,1664 (1) (2020); https://doi.org/10.1088/1742-6596/1664/1/012009
[43] O. M. Abdulmunem, A. M. Jabbar, S. K. Muhammad, M. O. Dawood, S. S. Chiad, N. F. Habubi, Journal of Physics: Conference Series,1660 (1), 012055 (2020); https://doi.org/ 10.1088/1742-6596/1660/1/012055
[44] E. H. Hadi, M. A. Abbsa, A. A. Khadayeir, Z. M. Abood, N. F. Habubi, and S.S. Chiad, Journal of Physics: Conference Series, 1664 (1), 012069 (2020); https://doi.org/ 10.1088/1742-6596/1664/1/012069
[45] Negar Khademi, M. M. Bagheri-Mohagheghi, Thermal Energy and Power Engineering. 2, 89-93(2013); https://doi.org/10.1016/j.jallcom.2013.05.057
[46] B. A. Bader, S. K. Muhammad, A. M. Jabbar, K. H. Abass, S. S. Chiad, N. F. Habubi, J. Nanostruct, 10(4): 744-750, (2020); https://doi.org/ 10.22052/JNS.2020.04.007
[47] F. H. Jasim, H. R. Shakir, S. S. Chiad,N. F. Habubi, Y. H. Kadhi,, Jadan, M., Digest Journal of Nanomaterials and Biostructures, 18(4), 1385–1393 (2023); https://doi.org/10.15251/DJNB.2023.184.1385
[48] H. T. Salloom, R. I. Jasim, N. F. Habubi, S. S. Chiad, M. Jadan, J. S. Addasi, Chinese Physics B, 30 (6), 068505 (2021); https://doi.org/10.1088/1674-1056/abd2a7
[49] S. S Chiad,, A. S. Alkelaby, K. S. Sharba,, Journal of Global Pharma Technology, 11 (7), 662-665, (2020); https://doi.org/10.1021/acscatal.1c01666
[50] Chiad, S.S., Noor, H.A., Abdulmunem, O.M., Habubi, N.F., Journal of Physics: Conference Series 1362(1), 012115 (2019); https://doi.org/10.1088/1742-6596/1362/1/012115
[51] J. Krysa, M. Zlamal, S. Kment and Z. Hubicka, The Italian Association of Chemical Engineering, 41, 379-484 (2014); https://doi.org/10.3303/CET1441064
[52] K. Y. Qader, E. H. Hadi, N. F. Habubi, S. S. Chiad, M. Jadan, J. S. Addasi, International Journal of Thin Films Science and Technology, 10 (1), 41-44 (2021); https://doi.org/ 10.18576/ijtfst/100107
[53] N. N. Jandow, M. S. Othman, N. F.Habubi, S. S. Chiad, K. A. Mishjil, I. A. Al-Baidhany, Materials Research Express, 6 (11), (2020); https://doi.org/10.1088/2053-1591/ab4af8
[54] M. D. Sakhil, Z. M. Shaban, K. S. Sharba, N. F. Habub, K. H. Abass, S. S. Chiad, A. S. Alkelaby, NeuroQuantology, 18 (5), 56-61 (2020); https://doi.org/10.14704/nq.2020.18.5.NQ20168
[55] E. S. Hassan, K. Y. Qader, E. H. Hadi, S. S. Chiad, N. F. Habubi, K. H. Abass, Nano Biomedicine and Engineering, 12(3), pp. 205-213 (2020); https://doi.org/10.5101/nbe.v12i3.p205-213
[56] M. S. Othman, K. A. Mishjil, H. G. Rashid, S. S. Chiad, N. F. Habubi, I. A. Al-Baidhany, Journal of Materials Science: Materials in Electronics, 31(11), 9037-9043 (2020); https://doi.org/10.1007/s10854-020-03437-0
[57] E. H. Hadi, D. A. Sabur, S. S. Chiad, N. F. Habubi, K., Abass, Journal of Green Engineering, 10 (10), 8390-8400 (2020); https://doi.org/10.1063/5.0095169
[58] K. Y. Qader, R. A. Ghazi, A. M. Jabbar, K. H. Abass, S. S. Chiad, Journal of Green Engineering, 10 (10), 7387-7398 (2020); https://doi.org/10.1016/j.jece.2020.104011
[59] R. I. Jasim, E. H. Hadi, S. S. Chiad, N. F. Habubi, M. Jadan, J. S. Addasi, Journal of Ovonic Research, 19 (2), 187 – 196 (2023)..
[59] K. S. Sharba, A. S. Alkelaby, M. D. Sakhil, K. H. Abass, N. F. Habubi, S. S. Chiad, Enhancement of urbach energy and dispersion parameters of polyvinyl alcohol with Kaolin additive, NeuroQuantology, 18 (3), 66-73 (2020); https://doi.org/10.14704/NQ.2020.18.3.NQ20152
[60] A. A. Khadayeir, E. S. Hassan, S. S. Chiad, N. F. Habubi, K. H. Abass, M. H. Rahid, T. H. Mubarak, M. O. Dawod, I. A. Al-Baidhany, Journal of Physics: Conference Series 1234 (1), 012014, (2019); https://doi.10.88/1742-6596/1234/1/012014
[61] Hassan, E.S., Mubarak, T.H., Chiad, S.S., Habubi, N.F., Khadayeir, A.A., Dawood, M.O., Al-Baidhany, I. A. , Journal of Physics: Conference Series, 1294(2), 022008 (2019); https://doi.10.88/1742-6596/1294/2/022008

[62] M.O. Dawood, S.S. Chiad, A.J. Ghazai, N.F. Habubi, O.M. Abdulmunem, AIP Conference Proceedings 2213, 020102,(2020); https://doi.org/10.1063/5.0000136
[63] J. Yang, J. H. Huang, D. Y. Fan, et al., Journal of Alloys and Compounds, 68 (9), 874-884 (2016); https://doi.org/10.1016/j.jallcom.2016.08.040
[64] H. H. Xiong, H. H. Zhang, H. N. Zhang, et al., Journal of Wuhan University of Technology-Mater. Sci. Ed, 33.(5), 1076-1081 (2018); https://doi.org/10.1007/s11595-018-1937-2
[65] S. A. Johansson, M. Christensen, G. Wahnström, Physical Review Letters, 95 (22), 226108 (2005); https://doi.org/10.1103/PhysRevLett.95.22610
[66] R. D. Suryavanshi, S. V. Mohite, A. A. Bagade, K. Y. Rajpure, Materials Science and Engineering: B, 248 (2019) 114386; https://doi.org/10.1016/j.mseb.2019.114386
[67] V.V. Malyshev, A.V. Eryshkin, E.A. Koltypin, A.E. Varfolomeev, A.A. Vasiliev, Sensors and Actuators B: Chemical 19 (1994) 434-436; https://doi.org/10.1016/0925-4005(93)01031-X
[68] M.R. Belkhedkar , A.U. Ubale, Y.S. Sakhare, N. Zubair, M. Musaddique, Journal of the Association of Arab Universities for Basic and Applied Sciences, 21, 38-44 (2016); https://doi.org/10.1016/j.jaubas.2015.03.001